Available online at www.sciencedirect.com
SCIENCE DIRECT®
International Journal of Heat and Fluid Flow 25 (2004) 274–287
International Journal of HEAT AND FLUID FLOW
www.elsevier.com/locate/ijhff

Subcooled boiling heat transfer and dryout on a constant temperature microheater

Tailian Chen, James F. Klausner *, Jacob N. Chung

Department of Mechanical and Aerospace Engineering, University of Florida, P.O. Box 116300, Gainesville, FL 32611-6300, USA

Abstract

An experimental study of single-bubble subcooled boiling heat transfer ($\Delta T_{sub} = 31.5$ K) on a small heater with constant wall temperature has been performed to better understand the boiling heat transfer associated with this unique configuration. The heater of 0.27 mm × 0.27 mm is set at different superheats to generate vapor bubbles on the microheater surface. For each superheat, the heater temperature is maintained constant by an electronic feedback control circuit while its power dissipation is measured at a frequency of 4.5 kHz. The single-bubble boiling is characterized by a transient bubble nucleation–departure period and a slow growth period. For the superheat range of 34–114 K in this study, at wall superheats below 84 K, the heater remains partially wetted following bubble departure and subsequent nucleation, and this period is characterized by a heat flux spike. At wall superheats above 90 K, the heater is blanketed with vapor following bubble departure and the heat flux experiences a dip during this period. At all superheats, the slow growth period is characterized by an almost uniform heat flux, and it has been observed that the heater surface is mostly covered by vapor. The unique heat transfer processes associated with boiling on this microheater are considerably different than those typically observed during boiling on a large heater.

Keywords: Boiling; Microheater; Ebullition; Transient heat flux; Dryout

1. Introduction

Applications of microtechnology commonly utilize components or systems with microscale fluid flow and heat and mass transfer. As the size of individual components shrinks and the length scale decreases, the transport mechanisms involved are typically outside the bounds covered by traditional theories and understanding. The development of new theories and the fostering of up-to-date physical understanding have fallen behind the progress of micromachining and manufacturing. Gad-el-Hak (1999) gave a complete review on the fluid mechanics of microdevices. He concluded that the technology is progressing at a rate that far exceeds the understanding of the fundamental transport phenomena in microdevices. Therefore, the study of microscale transport has become an integral part in, not only understanding the performance and operation of miniaturized systems, but also in designing and optimizing new devices.

Rule and Kim (1999) developed a heater array (2.7 mm × 2.7 mm), which consisted of 96 small constant temperature heaters. They presented space and time-resolved data for nucleate boiling, critical heat flux and transition boiling. Specifically, the outside edge heaters were found to have higher heat fluxes than those of the inner heaters.

Rainey and You (2001) reported an experimental study of pool boiling heat transfer using flat, microporous-enhanced square heater surfaces with three different sizes immersed in saturated FC-72. Results of the plain surface measurements showed that the nucleate boiling performance is dependent on heater orientation. The nucleate boiling curves of the microporous-coated surfaces were found to collapse to one curve showing insensitivity to heater orientation.

Bode et al. (1999) observed secondary bubble nucleation, in highly subcooled boiling. They claimed that secondary nucleation is initiated by the collapse of a large initial single bubble formed from an artificial nucleation site, accompanied with the generation of acoustic waves.

* Corresponding author. Tel.: +1-352-392-3506; fax: +1-352-392-1071.
E-mail address: klaus@ufl.edu (J.F. Klausner).

0142-727X/$ - see front matter © 2003 Elsevier Inc. All rights reserved.
doi:10.1016/j.ijheatfluidflow.2003.11.014

Hijikata et al. (1997) investigated boiling phenomena on microheaters of 50 μm and 100 μm maintained at constant heat flux. They observed that at low heat flux, the heater temperature changes periodically as bubbles grow and depart. However, at high heat flux, the periodic heater temperature variation is absent as a portion of the heater surface is always dried out.

The current paper presents an experimental study of boiling on a microheater that is maintained at constant temperature while the transient heat flux is measured. The heater size is on the same order as those used by Hijikata et al. (1997).

In order to avoid confusion, degrees Celsius are used when referring to temperature levels in the system and degrees Kelvin are indicated when referring to a temperature difference.

2. Experimental system

2.1. Microheater and temperature control circuit

The heater used in this experiment is one of many heaters on a heater array. Each heater is a platinum resistance element with a size of about 270 μm × 270 μm, and a nominal electrical resistance of 750 Ω at room temperature. It has a serpentine pattern shown in Fig. 1. Each-constant temperature heater is individually controlled by an electronic feedback circuit shown in Fig. 2. The heater array is fabricated on a quartz wafer using standard VLSI electronics fabrication technology. The material and manufacturing details, electronic feedback circuit for temperature control, and heater calibration were discussed previously by Rule and Kim (1999) and Chen and Chung (2002).

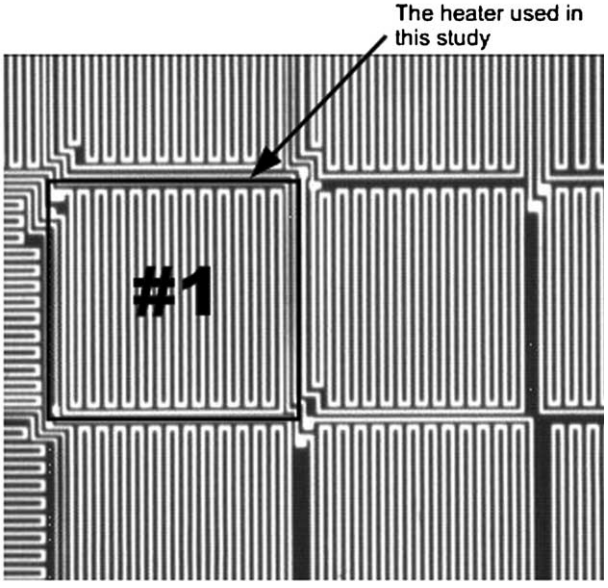

Fig. 1. A portion of the heater array showing the serpentine pattern of each heater.

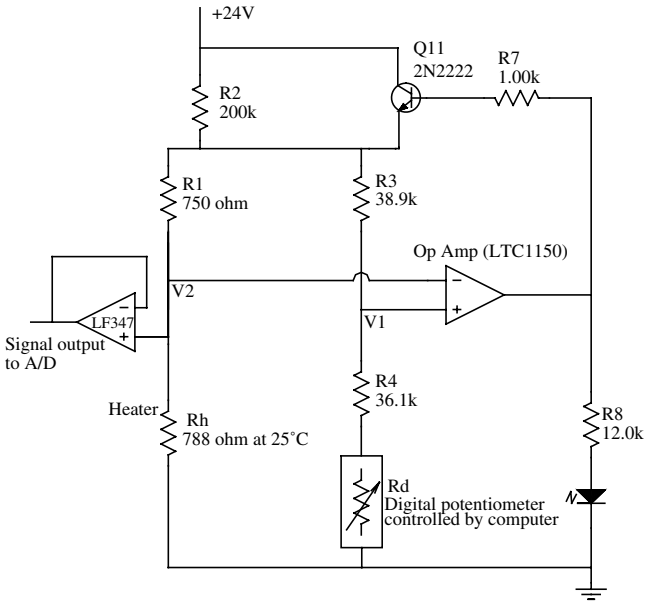

Fig. 2. The electronic circuit for temperature control.

2.2. Boiling conditions

The present experiment uses FC-72 as the boiling fluid. FC-72 is widely used in electronics cooling. Since it is dielectric, electrical conduction between the heaters through the bonding wires can be avoided and each heater can be individually controlled. The bulk fluid is maintained at ambient conditions (1 atm and 24.5 °C), and its corresponding saturation temperature is 56 °C. Therefore, there is a moderate degree of subcooling, $\Delta T_{sub} = 31.5$ K, for all the experiments performed. In the current experiment, a single microheater (marked as #1 in Fig. 1) is heated to produce vapor bubbles. The experiment is initiated by setting the microheater at a low temperature of 50 °C, where only natural convection occurs. Then the temperature of the heater is incremented by 5 K until the superheat reaches 114 K. For each increment, the heat dissipation by the heater is obtained with the data acquisition system by measuring the voltage across the heater. In order to explore the effects of dissolved gas on boiling heat transfer, boiling experiments have been performed for two cases. One case is when FC-72 is fully gas-saturated, and the other case is when FC-72 is fully degassed. In both cases, the bulk liquid is maintained at ambient conditions.

2.3. Data acquisition and visualization

The data acquisition system consists of two A/D boards (Measurement Computing CIO-DAS48) and a D/A board (Measurement Computing CIO-DIO48)

installed in a PC. The two A/D boards are used to acquire data and the D/A board is used to interface the computer signal with the electronic feedback system. The sampling rate in this experiment is about 4.5 kHz. The bubble visualization includes both bottom and side views. The transparent nature of the heater substrate makes it possible to visualize the boiling process from below. The setup of the experiment is shown in Fig. 3.

A high-speed digital camera (*Motion* Scope PCI 8000S) is used to take images at 1000 fps with a pixel resolution of 240×210. The bubble visualization is performed using the shadowgraph technique, in which the bubbles are illuminated from one side while the images are taken from the other side.

3. Data reduction

3.1. Heat transfer with boiling

By knowing the heater electrical resistance, the total heat dissipation rate from the heater, q''_{raw1}, is obtained by directly measuring the voltage across the heater. The heat transfer path is shown in Fig. 4(a). It includes the heat conduction to the substrate q''_{cond1}, the radiation to the surroundings, q''_{rad1}, and the boiling heat transfer to the liquid above the substrate, q''_{boil}, which could be a complex combination of heat transfer due to phase change, microconvection, and natural convection. Due to the small heater size, the size effect is important. As a single bubble is formed on the heater, the portion of heat transfer responsible for bubble growth has two possible heat transfer paths. One of them is direct evaporation of the liquid microlayer that resides above the heater surface and beneath the bubble. The other path is lateral conduction through the substrate that superheats a liquid layer in the vicinity of the heater substrate and liquid/vapor interface. The superheated liquid layer in turn supplies the energy required for evaporation along the bubble dome. During different portions of the growth period, the magnitude of heat transfer via these different paths changes considerably.

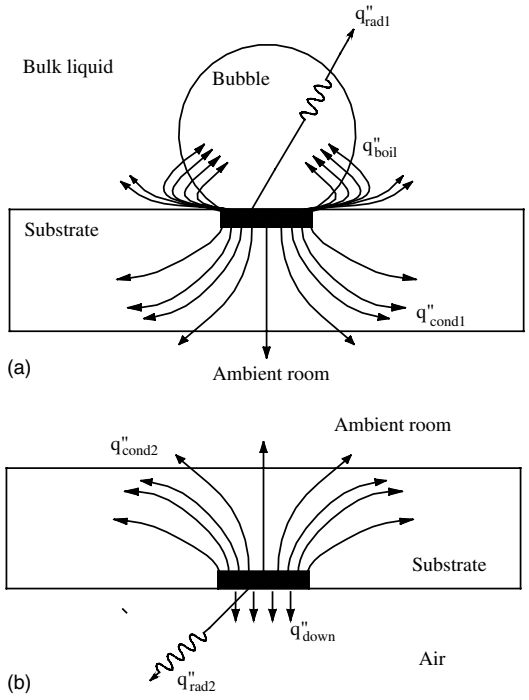

Fig. 4. Heat transfer paths from the heater: (a) with boiling and (b) without boiling.

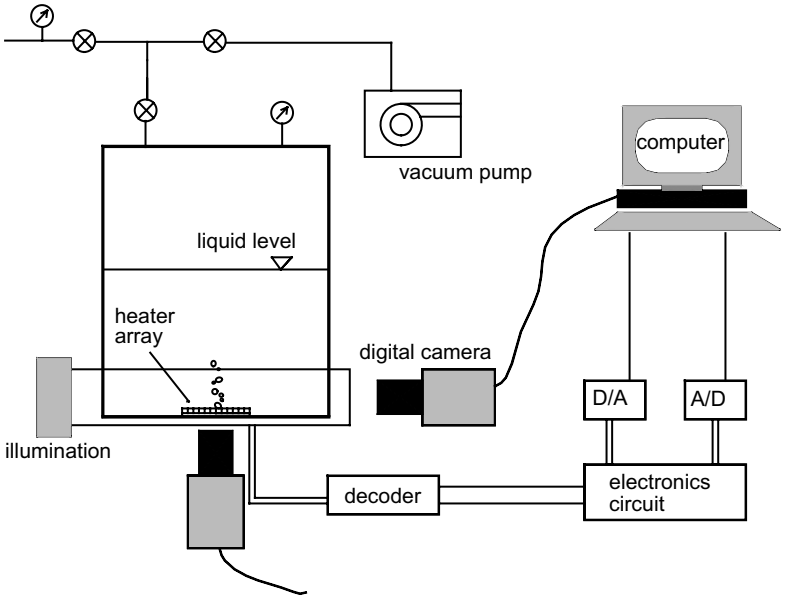

Fig. 3. Schematic diagram of experimental apparatus.

For the purpose of data reduction, these different heat transfer paths for bubble growth are not distinguished and are simply lumped into q''_{boil}. Therefore, the measured raw heat flux may be partitioned as

$$q''_{raw1} = q''_{cond1} + q''_{boil} + q''_{rad1}. \quad (1)$$

3.2. Data reduction procedure

The data reduction procedure is designed to evaluate q''_{boil}. The method is as follows. Following a boiling experiment, the boiling chamber is turned upside down, so that the heater is separated from the liquid FC-72. In this situation, the heater is set at the same temperatures as those encountered in the boiling experiment. For each temperature, the heater is allowed 20–30 minutes to reach steady state. Then the total heat dissipation rates are measured. The heat transfer path in this situation is shown in Fig. 4(b), and the total heat dissipation rate is expressed as

$$q''_{raw2} = q''_{cond2} + q''_{rad2} + q''_{down}, \quad (2)$$

where q''_{cond2} is the conduction heat flux to the substrate, q''_{rad2} is the radiation heat flux from the heater and q''_{down} is the conduction heat transfer downwards to the FC-72 vapor in the fully degassed case and to the mixture of air and FC-72 vapor in the fully gas-saturated case.

Because the heater is maintained at constant temperature by the electronic feedback system, the conduction heat transfer q''_{cond1} in Eq. (1) and q''_{cond2} in Eq. (2) are independent of the state of fluid above the heater. Since the heater is held at the same temperature for both operating conditions, $q''_{cond1} = q''_{cond2}$.

From Eqs. (1) and (2), the boiling heat flux, q''_{boil} can be determined as follows:

$$q''_{boil} = q''_{raw1} - q''_{raw2} + q''_{rad2} - q''_{rad1} + q''_{down}. \quad (3)$$

The only difference between the q''_{rad1} and q''_{rad2} is the radiation medium. For q''_{rad1}, the medium is FC-72 vapor inside the bubble and liquid outside the bubble, and for q''_{rad2}, the medium is air and FC-72 vapor. For both cases, the radiation media are essentially non-participating and can be neglected in the analysis. To obtain the value of q''_{boil} in Eq. (3), the conduction heat flux q''_{down} must be evaluated. Without the exact data for thermal conductivity of FC-72 vapor, its value is assumed equal to that of air, and q''_{down} has been evaluated using FEMLAB. The result shows that the conduction heat flux ranges from 1.27 to 2.5 W/cm^2 for heater temperatures ranging from 100 to 170 °C, which covers the temperature range in the current study. Thermal conductivity of FC-72 liquid is very small, only about twice that of air at the same temperature. The thermal conductivity of FC-72 vapor is significantly smaller than that of the liquid and thus the conduction heat flux, q''_{down}, should be even smaller than that estimated using FEMLAB. Since q''_{down} is computed to be negligibly small, the boiling heat transfer can be simply obtained from

$$q''_{boil} = q''_{raw1} - q''_{raw2}. \quad (4)$$

Here q''_{boil} is understood to be the cumulative heat flux from the heater due to phase change, microconvection, and natural convection.

3.3. Uncertainty analysis

The uncertainties in this experiment include those from the heater temperature and heat flux measurements. The uncertainty sources from the heater temperature are estimated as follows: oil temperature fluctuation during calibration, $\varepsilon_{T1} = +0.5$ K; discrete resistance increment of digital potentiometer, $\varepsilon_{T2} = +0.05$ K; drift of offset voltage V_{off} of the Opamp, $\varepsilon_{T3} = +0.1$ K; temperature fluctuation during boiling, especially during the vapor–liquid exchange process, $\varepsilon_{T4} = +0.01$ K. Thus, the overall temperature uncertainty is estimated by adding up the uncertainties from each source, which yields an uncertainty of about 0.66 K. The uncertainty sources associated with the boiling heat flux are summarized as follows: wiring resistance from A/D boards to heater pads, $\varepsilon_{V1} = 5\%$; resolution of A/D boards, $\varepsilon_{V2} = 0.03\%$; voltage divider, $\varepsilon_{V3} = 1.02\%$. They all come from the uncertainty of the acquired voltage from the heater. Thus, the total uncertainty for the voltage is: $\varepsilon_V = \varepsilon_{V1} + \varepsilon_{V2} + \varepsilon_{V3} = 5\% + 0.03\% + 1.02\% = 6.05\%$. The overall uncertainty for the heat flux has been estimated by using the method of Kline and McClintock (1953) to be approximately 0.5%.

4. Experimental results and analysis

4.1. Time-resolved heat flux history for a typical bubble cycle

For the superheat range of interest in the fully gas-saturated experiment, the time-resolved heat flux history shows that in one bubble cycle, there are two distinct growth periods. One is the transient nucleation–departure period, and the other one is the stable bubble slow growth period. For the nucleation–departure period, at superheats below 84 K, the nucleation–departure period produces a spike in the heat flux, with significant heat flux variation; at superheats above 90 K, a dip in heat flux is observed during the nucleation–departure period. For purposes of discussion, the superheat range is divided into two regimes: Regime I for superheat range 34–84 K and Regime II for 90–114 K based on the different heat transfer characteristics. For the slow bubble growth period, both in Regime I and Regime II, the heat flux level remains relatively flat. The heat flux

histories in a typical bubble cycle for superheats of 44 and 104 K have been shown in Fig. 5 to depict the distinct Regimes I and II. At $\Delta T_{sat} = 44$ K, a typical bubble cycle includes stages from [A] through [F] marked on Fig. 5(a). [A] corresponds to a large spike, which takes place during the bubble departure process. When the preceding bubble departs, the heater is rewetted by the subcooled bulk fluid. As will be discussed later, the nucleation of small bubbles and their coalescence, together with the turbulent microconvection induced by this vapor–liquid exchange, leads to the heat flux spike. [B] represents the moment when the succeeding bubble starts to grow after the vapor–liquid exchange. As the new bubble grows, the three-phase contact line expands outward as the heater surface begins to dry out. The bubble growth results in a larger dry area on the heater surface and thus the heat flux is decreasing. The low heat flux period indicated by [C], [D], and [E] corresponds to the slow growth period of the bubble. This period is characterized by total dryout of the heater surface, and the main heat transfer path is from the surrounding substrate to the superheated liquid, which supplies energy for bubble growth. The microlayer observed in classical boiling is non-existant during this growth stage. As the bubble size reaches a threshold the buoyancy force becomes comparable to the forces holding the bubble to the surface, and bubble necking is initiated. During the necking process, the contact line starts to shrink, and the dryout area starts to decrease. Thus it was observed that the heat flux started to increase slightly with some oscillation of small amplitude. Finally, the buoyancy force is large enough [F] to detach the bubble from the heater surface, and then another bubble ebullition cycle begins. For $\Delta T_{sat} = 104$ K, typical bubble cycles include stages [A′] through [F′] shown in Fig. 5(b). [C′]–[D′]–[E′] represent the slow growth period, [E′]–[F′] results from a stretching process when the bubble grows large, but not large enough to detach from the surface. [A′] and [B′] correspond to the moment of departure, and the detailed analysis for this period will be given later.

Visualization of a bubble during the slow growth period for $\Delta T_{sat} = 44$ K is shown in Fig. 6, which is visualized from the bottom of the heater surface using illumination from the top of the bubble. Each image in Fig. 6 is marked with a relative time when the images are taken; the time is not synchronized with Fig. 5(a). For each image, the inner transparent circular area results from the dry area of the heater. The inner white square denotes the border of the microheater. The outer diameter of the black annulus is the edge of the bubble. During the slow growth period, the bubble covers the whole heater surface and starts to shrink at 3.41 ms when bubble necking is initiated as part of the departure process. Fig. 7 shows the images for the bubble nucleation–departure period for $\Delta T_{sat} = 44$ K. It is seen that a single bubble forms following a departing bubble and it is noteworthy that, during this period, the heater

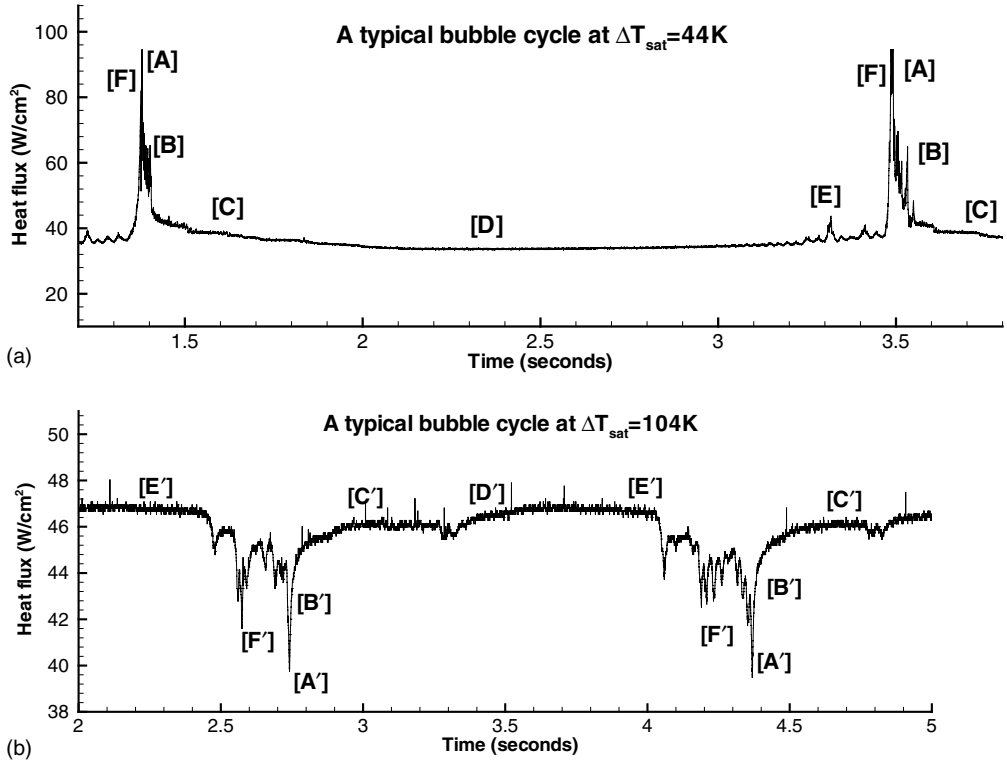

Fig. 5. Heat flux history during one typical bubble cycle at two different superheats: (a) $\Delta T_{sat} = 44$ K and (b) $\Delta T_{sat} = 104$ K.

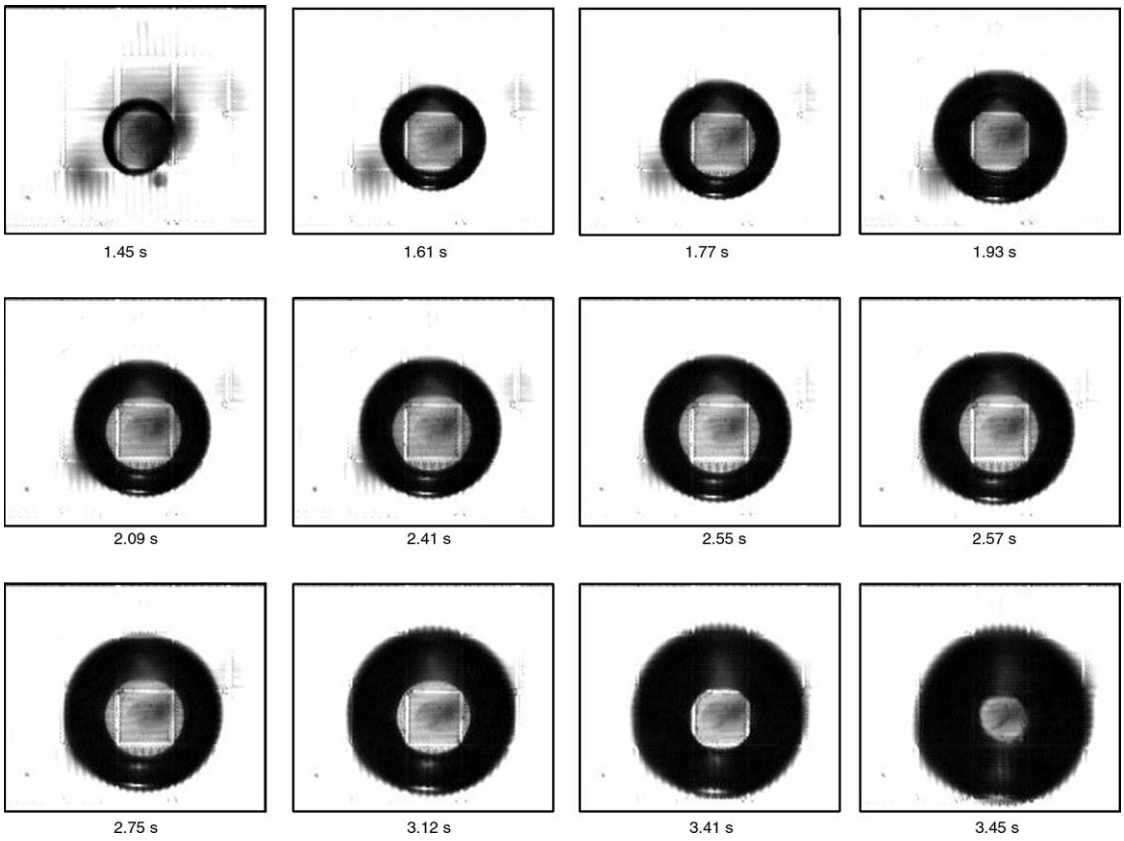

Fig. 6. Bottom view for the slow growth period of a typical bubble cycle at $\Delta T_{sat} = 44$ K.

surface remains partially wetted, as shown at 1–2 ms in Fig. 7.

4.2. Heat flux variation with heater dry area

To further examine the dry area change following bubble departure and its influence on the heat flux, Fig. 8 shows the heat flux history for $\Delta T_{sat} = 44$ K. The degree of rewetting is indicated for various intervals. At this superheat, just after the bubble departs, the heater surface is about 100% rewetted with a corresponding heat flux spike. As the bubble grows, its dry area spreads out and covers almost 100% of the heater surface, resulting in a low and flat heat flux. In between these two regimes, there is a strong fluctuation period that is a result of the bubble's rapid growth and oscillation. The heat flux spike is caused by the formation of secondary microbubbles and their coalescence. This will be even clearer as the bubble jetting phenomenon recorded during this experiment is examined. It is occasionally observed that there exists bubble jetting from the heater surface in two or three typical bubbling cycles. During the bubble jetting period, microbubbles nucleate on the heater surface and depart directly without merging into a single bubble. It is observed to last 0.1–0.2 s each time before a new single bubble is formed on the heater. Fig. 9 shows the heat flux history for a six-second window, which includes three bubble departing-nucleation processes. Fig. 9(a) shows the entire six-second window and Fig. 9(b) and (c) show two of the processes on an expanded time scale. The corresponding visualization for Fig. 9(b) has been shown in Figs. 10 and 11. It is observed that during the bubble jetting process, the heat flux remains as high as the heat flux spike during the regular single-bubble formation and falls off sharply as single-bubble growth takes over. The bubble jetting is characteristic of a chaotic bubble nucleation, merging, and departure process with the accompaniment of acoustic waves. During the bubble jetting process, small bubbles on the heater grow, merge, and depart until a merged bubble remains attached to the heater and small bubbles around it merge to form a single large bubble. The single bubble inhibits the bubble jetting by absorbing the small bubbles around it, and at the same time the microlayer beneath the bubble is dried out. Thus, the heat flux drops quickly as the single bubble enters the slow growth period.

For $\Delta T_{sat} < 84$ K in Regime I, it has been observed that single-bubble formation on the heater is always initiated with nucleation of small bubbles and their coalescence, which result in a higher heat flux. The delay

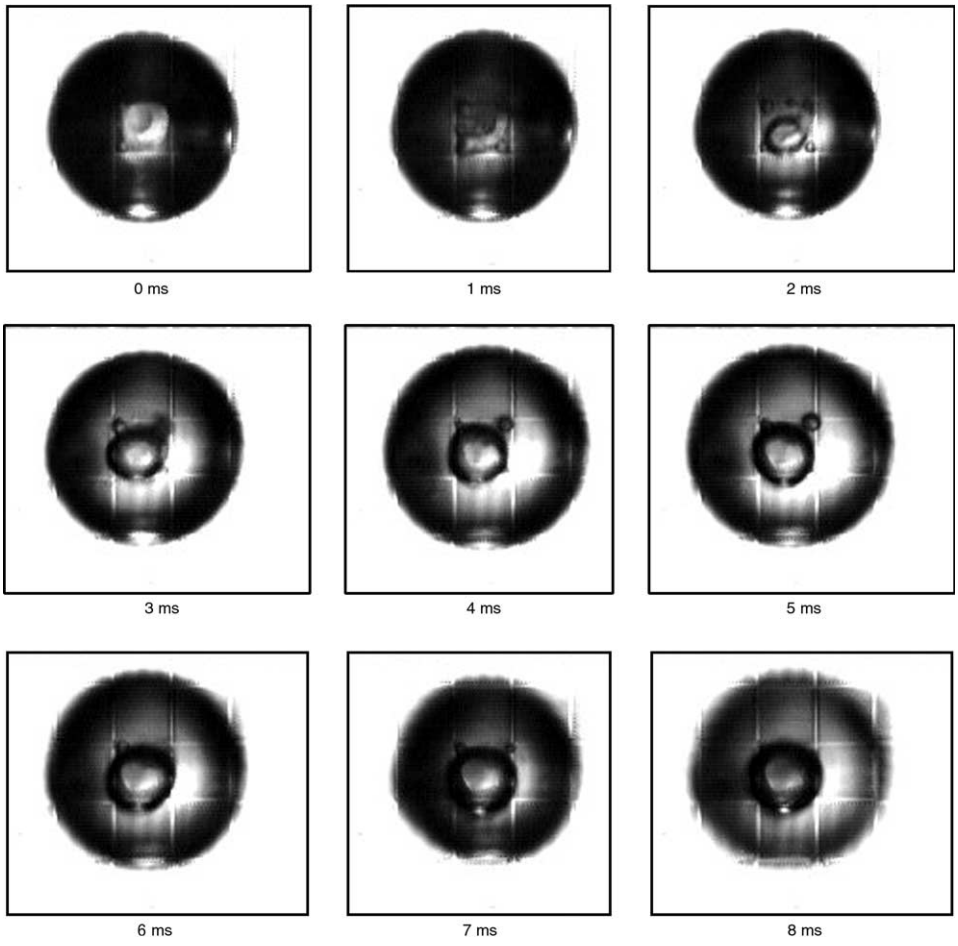

Fig. 7. Visualization of the bubble departure–nucleation process at $\Delta T_{sat} = 44$ K.

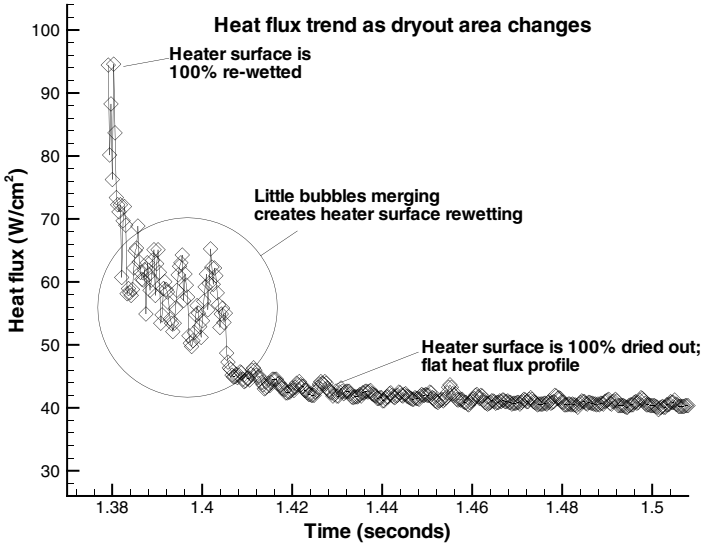

Fig. 8. Heat flux decrease as heater dry area increases.

time, when a merged bubble is sustained on the heater and absorbs other small bubbles, is what distinguishes the bubble jetting and regular single-bubble formation. A similar phenomenon was observed by Bode et al.

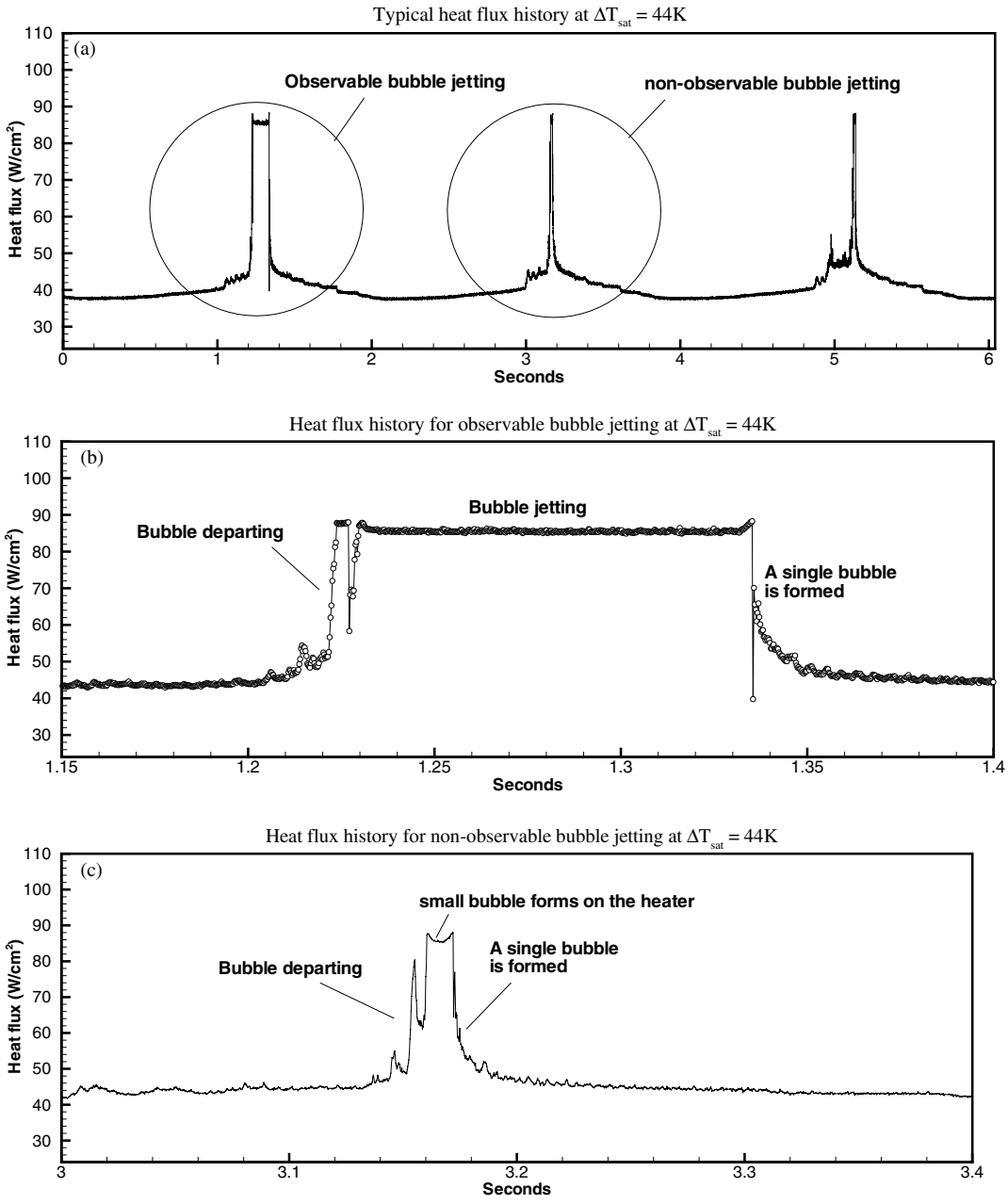

Fig. 9. Heat flux traces corresponding to the bubble jetting process.

(1999) who generated a single bubble from an artificial nucleation site on a much larger heater than that used in the current work. In their experiment, the heater was maintained at constant heat flux. They explained the nucleation of small bubbles to be a result of a secondary nucleation process initiated by the collapse of a departing bubble in subcooled liquid. As will be considered later, the necking phenomenon that occurs during the bubble departure process, shrinks the dry area and leaves leftover vapor on the heater surface. Whether or not this leftover vapor is subject to secondary nucleation remains for further analysis. The occurrence of bubble jetting is occasional and not periodic.

4.3. Time-resolved heat flux at different superheats

The time-resolved heat flux traces at eight different heater superheats are shown in Fig. 12, for superheats 44–74 K in Regime I, and for superheats 84–114 K in Regime II. It is observed that, in Regime I, a heat flux spike is produced during the bubble departure–nucleation process, as was discussed in detail in preceding sections. The magnitude of the heat flux spike decreases

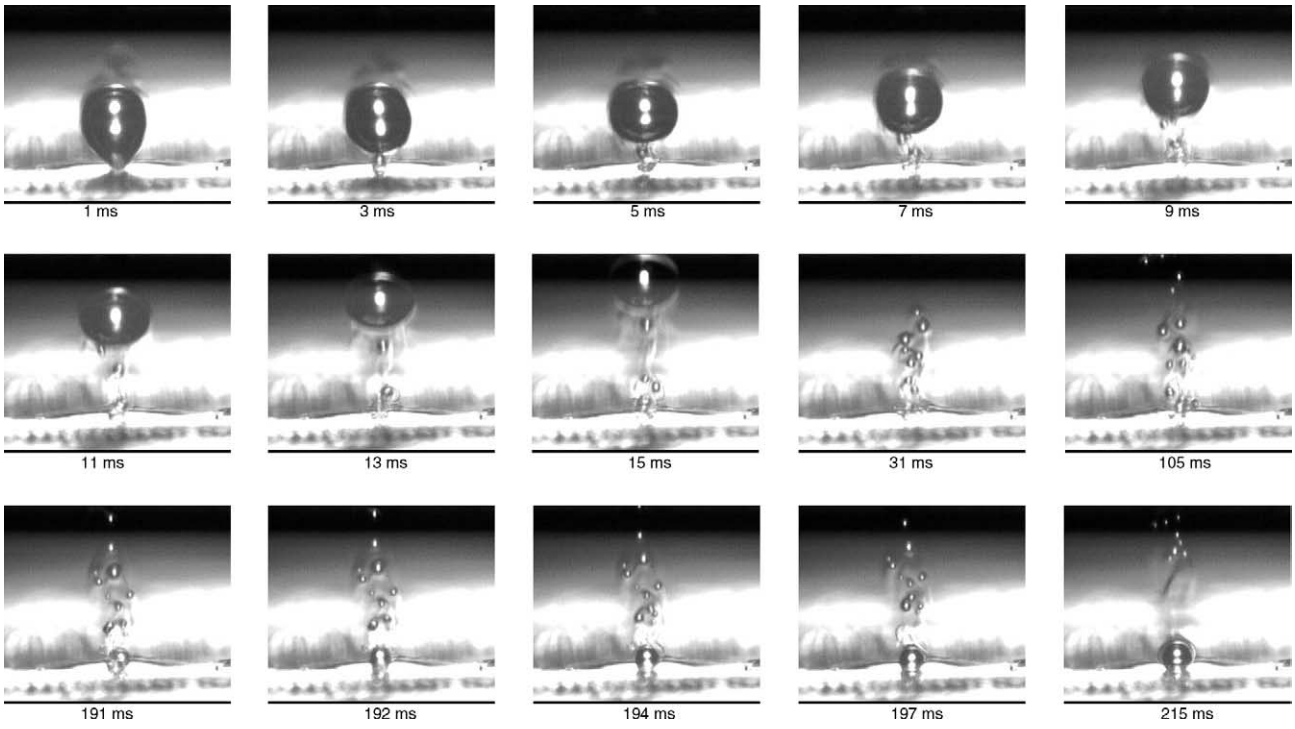

Fig. 10. Side view of the chaotic bubble jetting process at $\Delta T_{sat} = 44$ K.

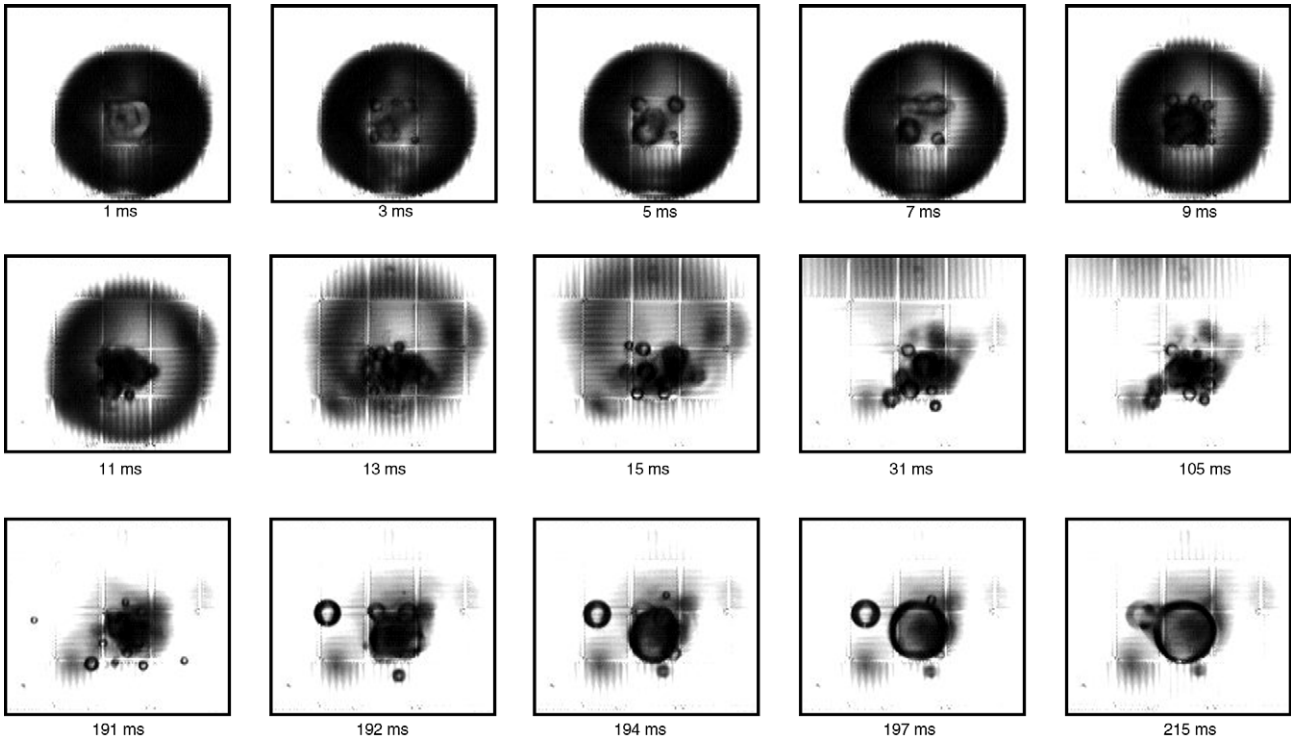

Fig. 11. Bottom view of the chaotic bubble jetting process at $\Delta T_{sat} = 44$ K.

with increasing superheat. In Regime II, the spike is no longer apparent. Instead of a heat flux spike, the departure–nucleation generates a heat flux dip.

According to homogeneous nucleation theory, as liquid is superheated to a threshold close to the critical temperature, spontaneous bubble growth will occur.

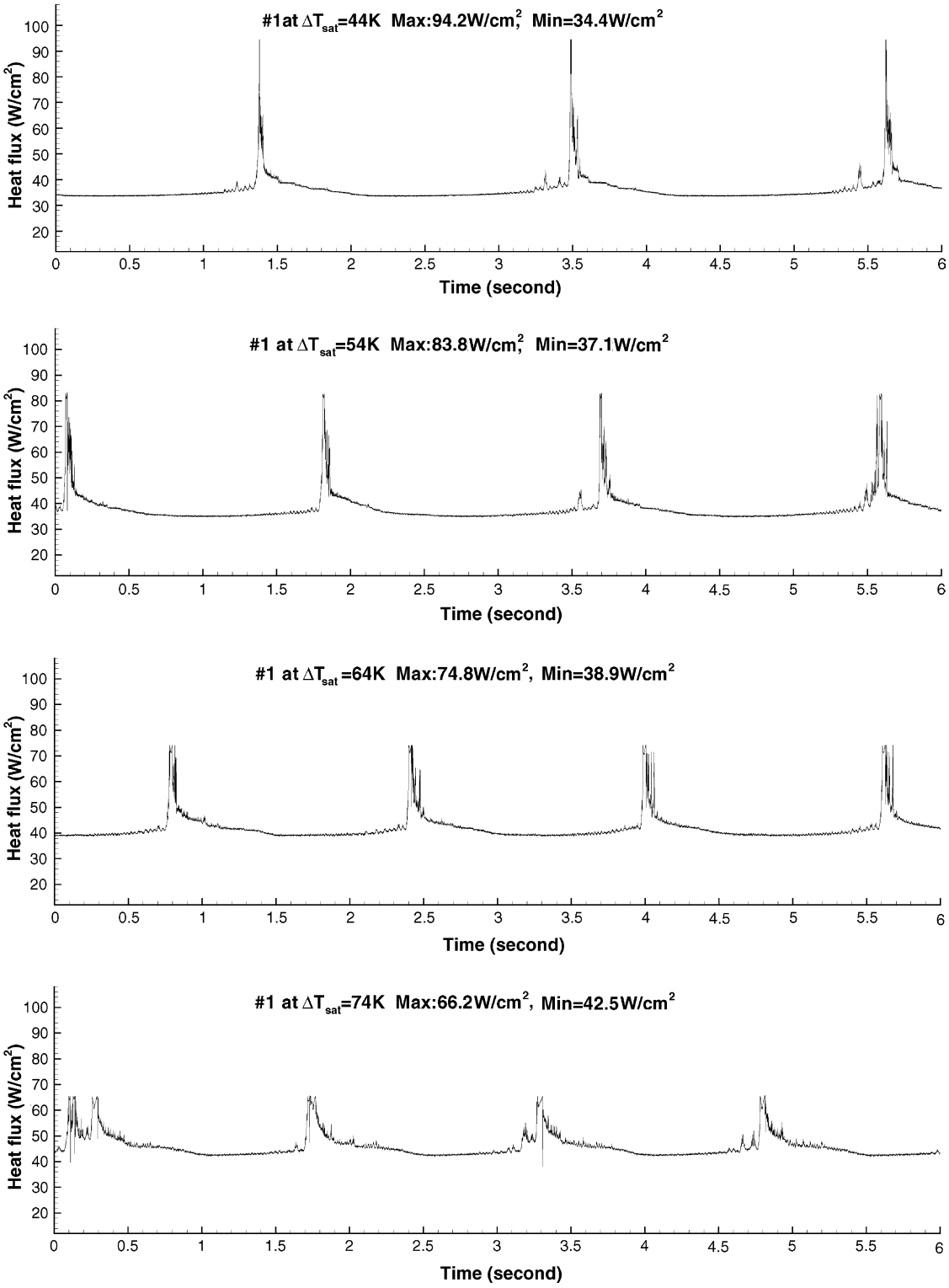

Fig. 12. Time-resolved heat flux traces at different superheats.

Using kinetic theory, the superheat limit can be related to the critical nucleation rate J_s ($m^{-3} s^{-1}$), which is the net flux of molecules from the liquid phase to the vapor phase.

Taking $J_s = 10^{12}$ $m^{-3} s^{-1}$, the threshold superheat for homogenous nucleation in FC-72 is computed to be 80 K using the method outlined by Carey (1992). This is indicative that homogenous nucleation may be

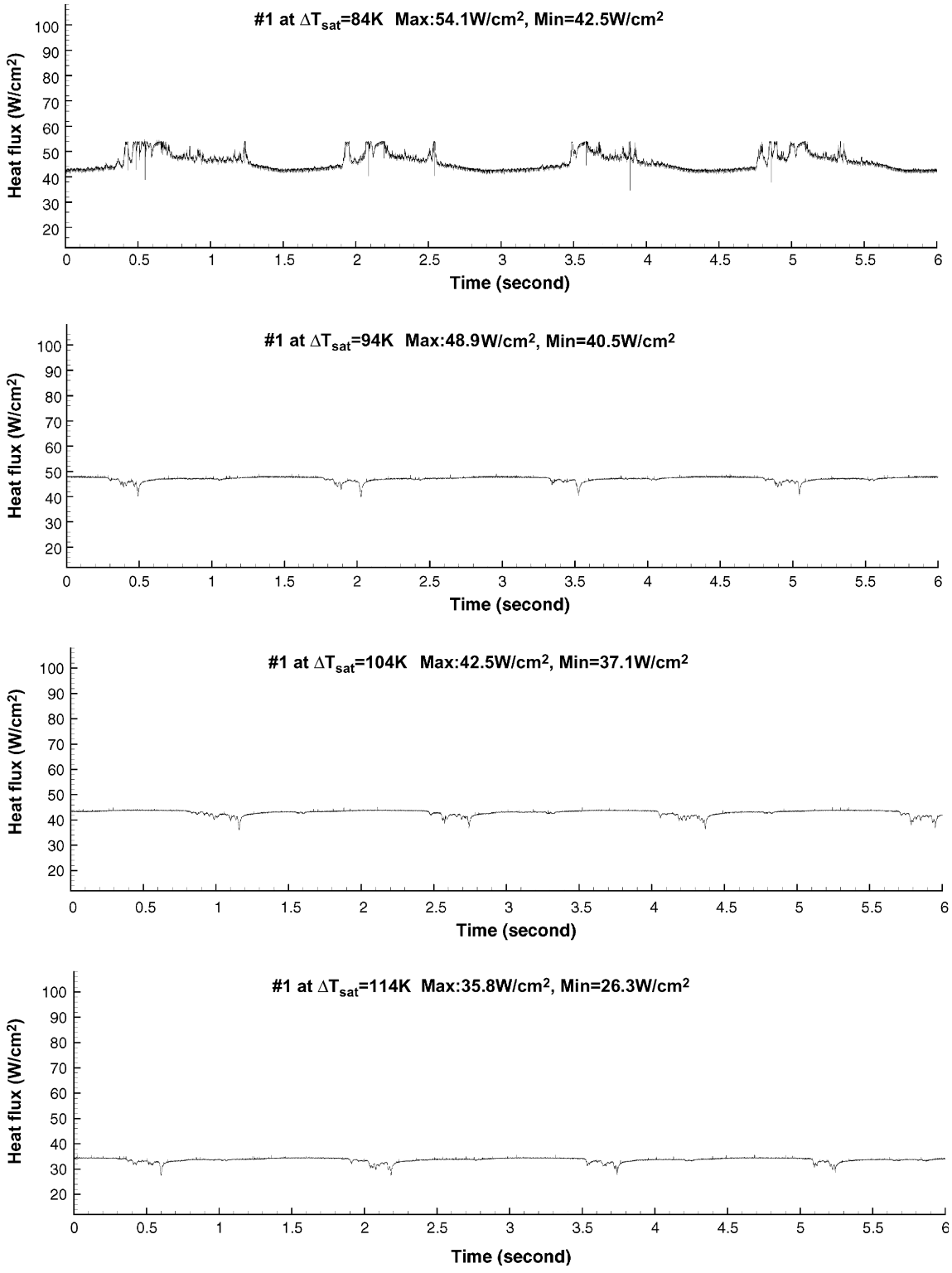

Fig. 12 (*continued*)

responsible for the transition to Regime II. In Regime II, as a bubble departs, the vapor left behind has no time to form a tiny bubble. Instead, homogeneous nucleation allows the vapor to immediately expand, covering a larger area beyond the heater surface such that part of the substrate outside the boundary of the heater is also covered by vapor. Yao and Henry (1978) have demonstrated that the onset of film boiling could be due to either a Taylor instability vapor removal limitation or homogeneous nucleation. For the current

boiling conditions, the critical Taylor wavelength is approximately 5 mm, which is an order of magnitude larger than the heater size. Since the Taylor wave cannot be sustained, it is reasonable that homogeneous nucleation is responsible for the vapor blanketing of the heater.

An attempt is made to explain the transition from Regime I to Regime II even though a precise physical understanding of the process has not been experimentally isolated. It is instructive to first consider those facts that have been experimentally observed: (1) in both regimes the bubble experiences necking during the departure process, (2) as the wall superheat is increased the dry area beneath the bubble expands, and (3) the transition from Regime I to Regime II corresponds to a transition from heterogeneous nucleation to homogeneous nucleation. Fig. 13 shows the heat flux variation during the departure–nucleation process on a refined time scale at four different wall superheats from 64 to 94 K. For superheats corresponding to 64 K and 74 K, the heat flux first increases rapidly at the outset of the departure–nucleation period followed by a small dip and a subsequent increase in heat flux. It is postulated that this observed behavior is caused by the following sequence of events. As the bubble begins necking during the departure process, the dry area beneath the bubble is reduced and the surface is rewetted, corresponding to an increase in heat flux. As the bubble departs, a vapor embryo is left behind that spreads over a portion of the heater surface, which corresponds to a small dip in heat flux. As the vapor embryo takes the shape of a bubble and begins to grow, the heat flux again increases. The magnitude of this dip increases with increasing superheat. It is believed that is the case because a larger quantity of vapor is left behind during the necking process with increasing superheat. This hypothesized sequence of events is shown graphically in Fig. 14(a). It is believed that the same dynamic process occurs during the departure–nucleation period in Regime II as shown schematically in Fig. 14(b). The difference is that since the wall superheat exceeds the homogeneous superheat limit, any vapor left behind during the departure process will instantaneously expand and blanket the entire heater surface and a portion of the surrounding substrate, causing a heat flux dip. As the vapor takes the shape of a vapor bubble, the dry area will be reduced and heat flux will rise slightly as the heat transfer process transitions to the slow growth behavior. Of course the vapor dynamics during the departure–nucleation period are highly transient and could not be discerned with the available apparatus.

q''_d is used to denote the peak heat fluxes corresponding to the bubble departure–nucleation period (heat flux spikes for $\Delta T_{sat} < 84$ K or heat flux dips for $\Delta T_{sat} > 90$ K). q''_s denotes the slow growth heat flux. Fig. 15 shows the variation of q''_d and q''_s with wall superheat.

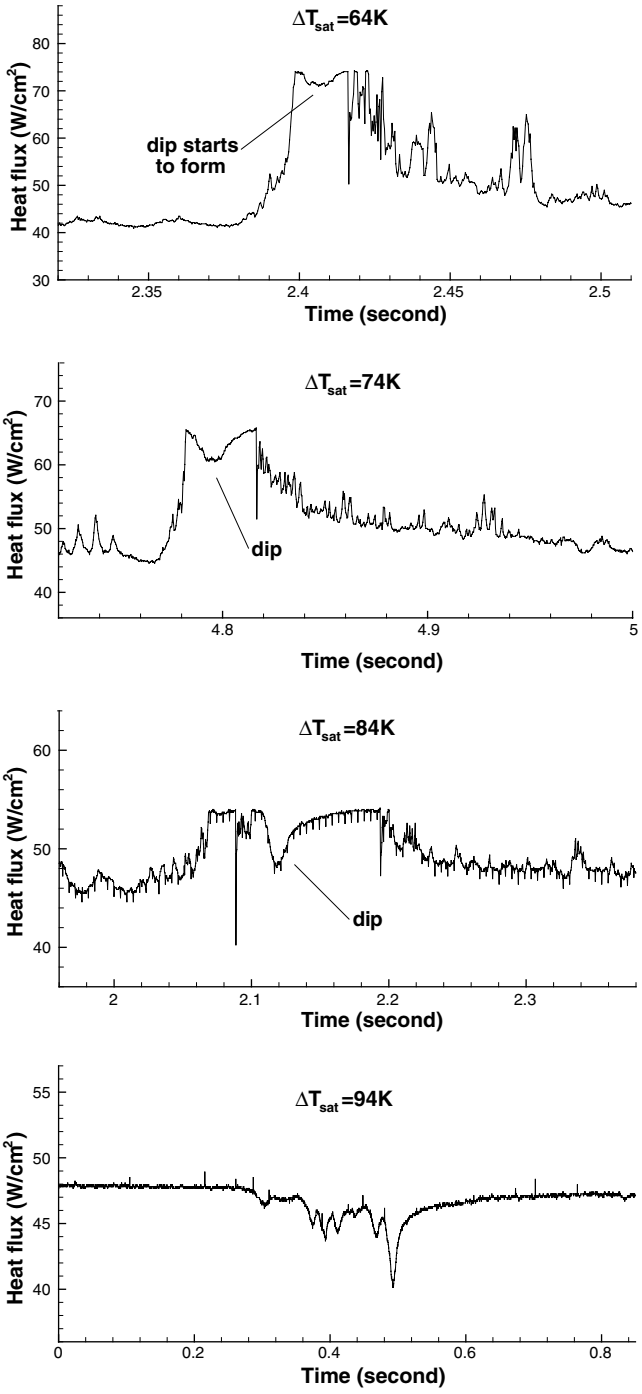

Fig. 13. A refined view of the heat flux history showing heat flux dips at different superheats.

It is observed that q''_d decreases with increasing superheat as explained above. q''_s does not vary substantially with superheat because the heater is already blanketed with vapor in this regime. When the heater surface is blanketed by vapor, the only viable heat transfer path is conduction to the surrounding substrate and to the liquid above it. Bubble growth can only proceed by extracting heat from the superheated liquid

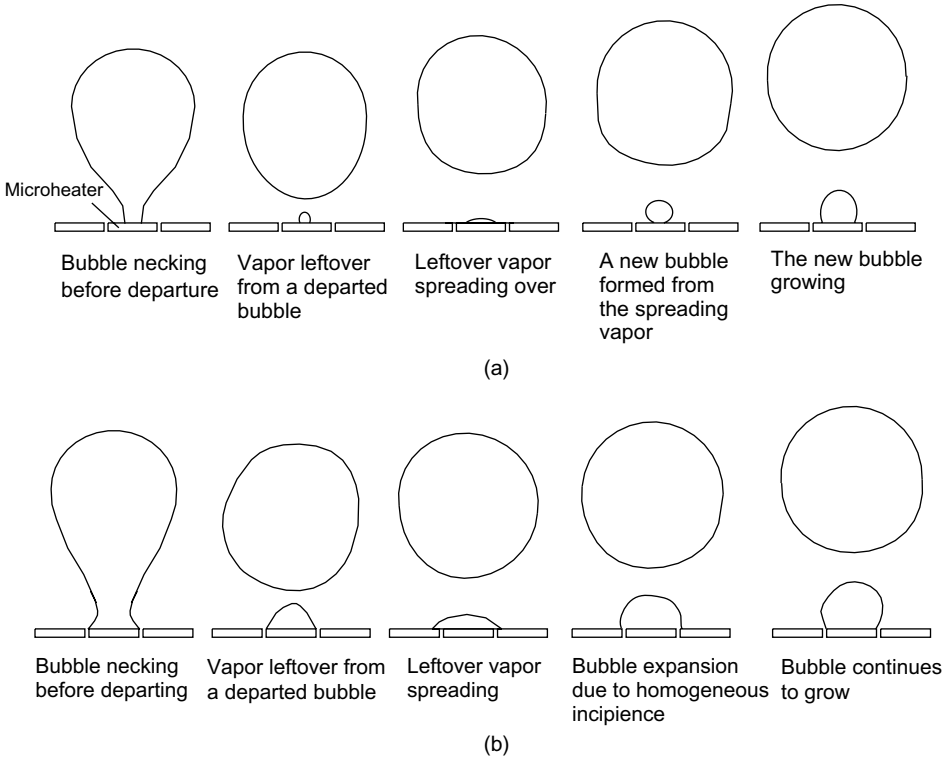

Fig. 14. Illustration of departure–nucleation process for wetted and vapor-blanketed regimes: (a) Regime I (partially wetted) and (b) Regime II (vapor blanketed).

layer adjacent to the bubble (see Liao et al., 2003). These results are consistent with those given by Hijikata et al. (1997) for constant heat flux microheaters of the same order in size, where they observed dryout of the heater as the bubble grows. Therefore, the large dryout area phenomenon associated with microheaters is not limited to the constant temperature heater surface used in these experiments.

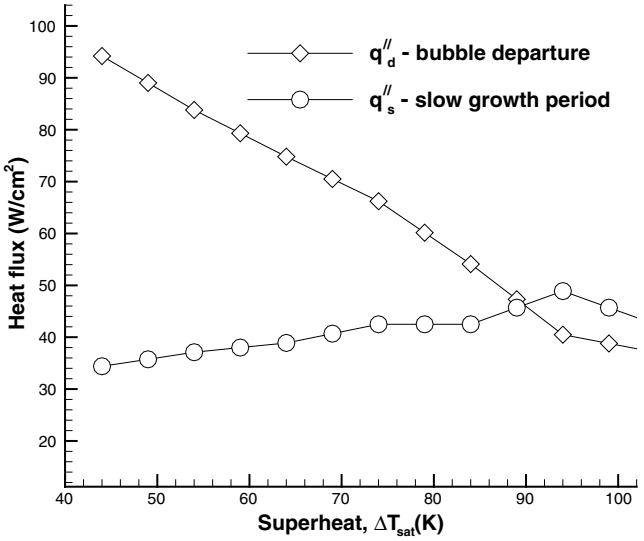

Fig. 15. q''_d and q''_s at various superheats.

4.4. Time-averaged boiling curve

The onset of nucleate boiling (ONB) for the fully gas-saturated liquid is found to be 54–59 K superheat, and it is about 5–10 K lower than for the fully degassed liquid. After the ONB, the degree of superheat was dropped to 34 K, which is the minimum superheat for stable boiling on the heater. Fig. 16 shows the two measured boiling curves for fully gas-saturated and fully degassed boiling, where the superheat covers a range from 34 to 114 K. They were obtained by evaluating the average heat fluxes for each superheat. For both cases, the experiment was repeated three times (3 runs). As shown in Fig. 16, the boiling curves exhibit the same trend. The heat flux for the fully gas-saturated case is about 10% higher than the fully degassed state at corresponding superheats. There are two distinct regimes associated with the boiling curves, Regime I and Regime II, which are separated by a peak heat flux at a superheat of about 90 K. In Regime I the heat flux increases with superheat, and in Regime II the heat flux decreases with superheat. The demarcation between the two regimes is governed by whether or not the microheater is rewetted following bubble departure and approximately corresponds to the homogeneous nucleation superheat. The two regimes correspond to those identified for time-varying heat flux.

It is interesting that the trend of the curves in Fig. 16 remains similar to the classical nucleate and transition

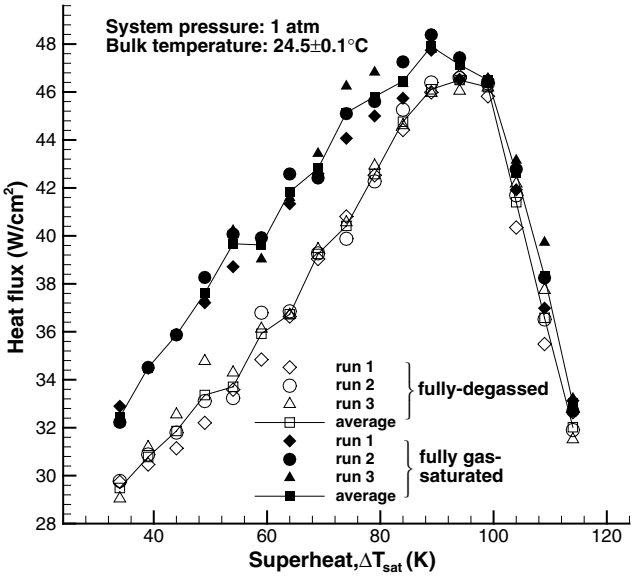

Fig. 16. Boiling curves for fully gas-saturated and fully degassed cases.

boiling curves identified by Nukiyama (1934). However, the fundamental boiling process for a single bubble on a microheater is considerably different than that for classical boiling on large heaters. Thus using an average representation for the complex heat transfer process should be done with caution.

5. Conclusion

An experimental study was performed to examine the heater dry area variation during single-bubble boiling on a constant-temperature microheater and the associated complex heat transfer process. Single-bubble boiling on a microheater is characterized by transient bubble nucleation–departure periods and slow growth periods. It is found that at superheats less than 84 K, the heater remains partially wetted during the bubble departure period. At superheats greater than 90 K, the heater surface is completely blanketed by vapor following bubble departure, and the homogeneous nucleation process dominates the bubble incipience. At all superheats, the heater is almost completely blanketed by vapor during the slow growth regime.

Acknowledgements

The technical assistance and fruitful discussions offered by Jungho Kim of the University of Maryland are greatly appreciated. This research was made possible by the Andrew H. Hines, Jr./Florida Progress Endowment Fund.

References

Bode, A., Kling, K., Schröder, J.J., Viertmann, M., 1999. Natural alternations in subcooled pool boiling heat transfer. In: Proceedings of Convective and Pool Boiling.

Carey, V.P., 1992. Liquid–vapor Phase Change Phenomena—An Introduction to the Thermodynamics of Vaporization and Condensation Processes in Heat Transfer Equipment. Taylor and Francis, Bristol, PA.

Chen, T., Chung, J.N., 2002. Coalescence of bubbles in nucleate boiling on microheaters. Int. J. Heat Mass Transfer 45, 2329–2341.

Gad-el-Hak, M., 1999. The fluid mechanics of microdevices—the Freeman Scholar Lecture. J. Fluids Eng. 121, 5–31.

Hijikata, K., Yamamoto, N., Takagi, S., 1997. Boiling heat transfer from a micro heater. In: Micro-electro-mechanical Systems (MEMS), DSC-vol 62/HTD-vol 354. ASME, pp. 135–142.

Kline, S.J., McClintock, F.A., 1953. Describing uncertainties in single-sample experiments. Mech. Engin. 75, 3–8.

Liao, J., Mei, R., Klausner, J.F., 2003. The influence of the bulk liquid thermal boundary layer on bubble growth in saturated nucleate boiling. In: Proceedings of the 5th International Conference on Boiling Heat Transfer, Montego Bay, Jamaica.

Nukiyama, S., 1934. The maximum and minimum values of heat transmittal from metal to boiling water under atmospheric pressure. J. Jpn. Soc. Mech. Eng. 37, 367–374.

Rainey, K.N., You, S.M., 2001. Effects of heater size and orientation on pool boiling heat transfer from microporous coated surfaces. Int. J. Heat Mass Transfer 44, 2589–2599.

Rule, T., Kim, J., 1999. Heat transfer behavior on small horizontal heaters during pool boiling of FC-72. J. Heat Transfer 121, 386–393.

Yao, S., Henry, R.E., 1978. An investigation of the minimum film boiling temperature on horizontal surfaces. J. Heat Transfer 100, 260–267.